1966 *Chem. Mater.* **2010,** *22,* 1966–1976
DOI:10.1021/cm903357q

CHEMISTRY OF MATERIALS
Article

Smart Core−Shell Hybrid Nanogels with Ag Nanoparticle Core for Cancer Cell Imaging and Gel Shell for pH-Regulated Drug Delivery

Weitai Wu,[†] Ting Zhou,[†] Alexandra Berliner,[†,§] Probal Banerjee,[†,§] and Shuiqin Zhou*,[†]

[†]*Department of Chemistry and* [§]*CSI/IBR Center for Developmental Neuroscience, The College of Staten Island, and The Graduate Center, The City University of New York, 2800 Victory Boulevard, Staten Island, New York 10314*

Received November 3, 2009. Revised Manuscript Received January 21, 2010

Multifunctional nanoparticles that can provide long circulation and specific accumulation, illuminate the targeted object, and intelligently dose the pathological zones will enable major advancements in diagnosis and therapy. To facilitate a simultaneous tumor-cell imaging and adequate local delivery to the tumor site, we develop core−shell structured hybrid nanogels (40−80 nm) composed of a Ag nanoparticle (NP) as core and smart gel of poly(*N*-isopropylacrylamide-*co*-acrylic acid) as shell. The pH-induced shrinkage of the nanogel increases the UV−vis absorption intensity and causes a blue shift of the surface plasmon bands of the Ag NP core. The smart nanogel can overcome cellular barriers to enter the intracellular region and light up the mouse melanoma B16F10 cells, including the nuclear regions. The surface property and concentrations of the hybrid nanogels influences their interactions with cells, resulting in different cell morphology and selective cell staining. The pH-responsive hybrid nanogels exhibit not only a high drug loading capacity but also a pH-controllable drug releasing behavior. Smart hybrid nanogels with optical and therapeutic functionality, designed by integration of functional building blocks, offer broad opportunities for biomedical applications.

1. Introduction

An exciting new trend in bio/nanotechnology is to develop novel multifunctional nanomaterials that are capable of combining imaging diagnostics, sensing, and controlled drug delivery for therapy.[1−5] Noble metals such as Ag and Au nanoparticles (NPs) possess unique optical properties, including surface-enhanced, distance-dependent, refractive index-dependent spectroscopic properties and antiphotobleaching properties[6−12] and thus have been extensively explored for optical markers in biodiagnostic imaging. For example, their tunable surface plasmon resonance and large scattering cross sections have been used for scattering-based imaging,[11−16] while their excellent antiphotobleaching properties have been applied for fluorescence-based cellular imaging under strong light illumination.[10,16−21] On the other hand, noble metal NPs are also being actively explored for drug

*To whom correspondence should be addressed. E-mail: shuiqin.zhou@csi.cuny.edu. Tel: 718-982-3897.

(1) Biju, V.; Itoh, T.; Anas, A.; Sujith, A.; Ishikawa, M. *Anal. Bioanal. Chem.* **2008**, *391*, 2469.
(2) Smith, A. M.; Duan, H.; Mohs, A. M.; Nie, S. *Adv. Drug Delivery Rev.* **2008**, *60*, 1226.
(3) Park, K.; Lee, S.; Kang, E.; Kim, K.; Choi, K.; Kwon, I. C. *Adv. Funct. Mater.* **2009**, *19*, 1553.
(4) Liong, M.; Kovochich, M.; Xia, T.; Ruehm, S. G.; Nel, A. E.; Tamanoi, F.; Zink, J. I. *ACS Nano* **2008**, *2*, 889.
(5) McCarthy, J. R.; Weissleder, R. *Adv. Drug Delivery Rev.* **2008**, *60*, 1241.
(6) Lim, I.-I. S.; Chandrachud, U.; Wang, L.; Gal, S.; Zhong, C. J. *Anal. Chem.* **2008**, *80*, 6038.
(7) (a) Contreras-Caceres, R.; Sanchez-Iglesias, A.; Karg, M.; Pastoriza-Santos, I.; Perez-Juste, J.; Pacifico, J.; Hellweg, T.; Fernandez-Barbero, A.; Liz-Marzán, L. *Adv. Mater.* **2008**, *20*, 1666. (b) Alvarez-Puebla, R. A.; Contreras-Caceres, R.; Pastoriza-Santos, I.; Perez-Juste, J.; Liz-Marzán, L. *Angew. Chem., Int. Ed.* **2009**, *48*, 138.
(8) (a) Conner, S. D.; Schmld, S. L. *Nature* **2003**, *422*, 37. (b) Verma, A.; Uzun, O.; Hu, Y. H.; Hu, Y.; Han, H.; Watson, N.; Chen, S.; Irvine, D. J.; Stellacci, F. *Nat. Mater.* **2008**, *7*, 588. (c) Goda, T.; Gota, Y.; Ishihara, K. *Biomaterials* **2010**, *31*, 2380; doi: 10.1016/j.biomaterials.2009.11.095.
(9) Elghanian, R.; Storhoff, J. J.; Mucic, R. C.; Letsinger, R. L.; Mirkin, C. A. *Science* **1997**, *277*, 1078.
(10) Geddes, C. D.; Gryczynski, I.; Parfenov, A.; Aslan, K.; Lakowicz, J. R. *Proc. SPIE-Int. Soc. Opt. Eng.* **2004**, *5329*, 276.
(11) Batista, P.; Pereira, E.; Eaton, P.; Doria, G.; Miranda, A.; Gomes, I.; Quaresma, P.; Franco, R. *Anal. Bioanal. Chem.* **2008**, *391*, 943.
(12) Wilson, R. *Chem. Soc. Rev.* **2008**, *37*, 2028.
(13) Song, K. H.; Kim, C.; Cobley, C. M.; Xia, Y. N.; Wang, L. V. *Nano Lett.* **2009**, *9*, 183.
(14) Lee, K. S.; El-Sayed, M. A. *J. Phys. Chem. B* **2006**, *110*, 19220.
(15) Schultz, D. A. *Curr. Opin. Biotechnol.* **2003**, *14*, 13.
(16) Xu, C.; Xie, J.; Ho, D.; Wang, C.; Kohler, N.; Walsh, E. G.; Morgan, J. R.; Chin, Y. E.; Sun, S. *Angew. Chem., Int. Ed.* **2008**, *47*, 173.
(17) Wang, H. F.; Huff, T. B.; Zweifel, D. A.; He, W.; Low, P. S.; Wei, A.; Cheng, J. X. *Proc. Natl. Acad. Sci. U.S.A.* **2005**, *102*, 15752.
(18) Durr, N. J.; Larson, T.; Smith, D. K.; Korgel, B. A.; Sokolov, K.; Ben-Yakar, A. *Nano Lett.* **2007**, *7*, 941.
(19) He, H.; Xie, C.; Ren, J. *Anal. Chem.* **2008**, *80*, 5951.
(20) (a) Schrand, A. M.; Braydich-Stolle, L. K.; Schlager, J. J.; Dai, L. M.; Hussain, S. M. *Nanotechnology* **2008**, *19*, 235104. (b) Dulkeith, E.; Niedereichholz, T.; Klar, T. A.; Feldmann, J.; von Plessen, G.; Gittins, D. I.; Mayya, K. S.; Caruso, F. *Phys. Rev. B* **2004**, *70*, 205424.
(21) Jiang, J.; Gu, H.; Shao, H.; Devlin, E.; Papaefthymiou, G. C.; Ying, J. Y. *Adv. Mater.* **2008**, *20*, 4403.

Published on Web 02/12/2010

delivery vectors under different surface functionalization.[22−26] A key attribute of drug delivery systems is their ability to regulate drug release, minimize side effects, and improve therapeutic efficacy of conventional pharmaceuticals.[27] Photothermal conversion in noble metal NPs increases the temperature locally, which can sensitize targeted cells to cytotoxic agents by increasing membrane permeability and blood vessel dilation.[28] If the photothermal therapy can be combined with chemotherapy, a much higher therapeutic efficacy is expected. However, the development of noble metal NP-based therapeutic systems with high drug loading capacity and stimuli-responsive release profile for the delivery of various generic pharmaceuticals remains a big challenge. The drug delivery vectors prepared from monolayer protected metal NPs usually provide low drug loading capacity,[22−26] although the photoregulated release can be achieved for photosensitive drugs.[25,26] Sershen et al.[29] have embedded the Au_2S/Au NPs in the surface layer of thermal sensitive hydrogel slabs to achieve high drug loading capacity and photothermally modulated drug release. However, the bulky hydrogel discs are not suitable for drug delivery carriers because the size of drug carrier particles less than 200 nm is desirable to increase their circulation time in blood.[30] Furthermore, for some applications, the drug carrier vehicles that can respond to a particular biostimulus such as pH change are preferred.

To integrate the multifunctions for imaging diagnostics and controlled drug release into one single system, Park et al.[31] have fabricated polymer−metal multilayer half-shell particles, in which the Mn and Au nanolayers were subsequently deposited onto the monolayers of biodegradable poly(lactide-*co*-glycolic acid) (PLGA) nanoparticles (~75 nm) that were spin-casted on a silicon substrate. In such a case, the metal nanolayers only cover half of the surface of the spherical PLGA particles to form a half-shell. While the PLGA particles function as a drug carrier for a model drug of rhodamine, the magnetic Mn nanolayer can serve as the contrast agents for magnetic resonance imaging (MRI) and the Au nanolayer can absorb the NIR irradiation to convert the light to heat for photothermally controlled drug release, respectively. Since Mn and Au nanolayers cover the half-shell of the drug-loaded

Scheme 1. Schematic Illustration of Drug-Loaded Core−Shell Hybrid Nanogels with the Smart Gel Shell Immobilized on the Ag NP Core for Integration of Tumor-Cell Imaging and pH-Triggered Drug Delivery

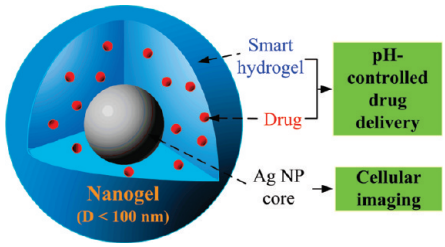

PLGA particles, the drug molecules can only be released through the uncovered half-surface of the PLGA particles.

In this work, we aim to develop a new class of core−shell structured multifunctional nanomaterials for integration of cellular imaging and pH-regulated drug delivery with a high drug loading capacity. Our strategy is based on the immobilization of a smart gel shell of poly(*N*-isopropylacrylamide-*co*-acrylic acid) [p(NIPAM-*co*-AA)] onto Ag NPs (see Scheme 1). While the Ag NP core can act as an optical identification code for tumor-cell imaging,[20] the p(NIPAM-*co*-AA) gel shell can serve as drug carriers with high loading capacity. The p(NIPAM-*co*-AA) gel shell can swell and shrink in response to pH change, which can not only modify the physicochemical environment of the embedded Ag NPs to manipulate the optical properties of the core but also change the mesh size of the gel shell to regulate the drug release behavior. pH-responsive microgels/nanogels offer unique advantages for polymer-based drug delivery systems: a tunable size, large surface area for bioconjugation, interior network structure for the incorporation of therapeutics, low side effects of drugs, and controllable release at a specific pH environment.[32a] Various pH-responsive polymer micro/nanogels have been explored to carry bioactive molecules such as drugs, proteins, carbohydrates, and DNA for controlled release.[32] Whereas photothermal triggered release is used in a passive way,[29,31] pH-responsive release herein involves an active role of the therapy. Many pathological processes in various tissues and organs such as cancer and cystic fibrosis are accompanied with a local pH decrease (acidosis). The pH responsive hybrid nanogel particles acting as drug delivery carriers should possess the ability to switch on and off for certain functions when necessary under the local stimuli of the target pathological zone such as cancer and cystic fibrosis that are associated with disruptions in acid/base homeostasis.[33] We have selected

(22) Boisselier, E.; Astruc, D. *Chem. Soc. Rev.* **2009**, *38*, 1759.
(23) Paciotti, G. F.; Myer, L.; Weinreich, D.; Goia, D.; Pavel, N.; McLaughlin, R. E.; Tamarkin, L. *Drug Delivery* **2004**, *11*, 169.
(24) Kim, C. K.; Ghosh, P.; Pagliuca, C.; Zhu, Z. J.; Menichetti, S.; Rotello, V. M. *J. Am. Chem. Soc.* **2009**, *131*, 1360.
(25) Cheng, Y.; Samia, A. C.; Meyers, J. D.; Panagopoulos, I.; Fei, B.; Burda, C. *J. Am. Chem. Soc.* **2008**, *130*, 10643.
(26) Agasti, S. S.; Chompoosor, A.; You, C. C.; Ghosh, P.; Kim, C. K.; Rotello, V. M. *J. Am. Chem. Soc.* **2009**, *131*, 5728.
(27) Peer, D.; Karp, J. M.; Hong, S.; Farokhzad, O. C.; Margalit, R. *Nat. Nanotechnol.* **2007**, *2*, 751.
(28) Rowe-Horwege, R. W. *Systemic Hyperthermia in Encyclopedia of Medical Devices and Instrumentation*, 2nd ed; Webster, J. G., Ed; John Wiley and Sons: New York, 2006; pp 42−62.
(29) Sershen, S. R.; Westcott, S. L.; Halas, N. J.; West, J. L. *J. Biomed. Mater. Res.* **2000**, *51*, 293.
(30) Alexis, F.; Pridgen, E.; Molnar, L. K.; Farokhzad, O. C. *Mol. Pharmaceutics* **2008**, *5*, 505.
(31) Park, H.; Yang, J.; Seo, S.; Kim, K.; Suh, J.; Kim, D.; Haam, S.; Yoo, K. H. *Small* **2008**, *4*, 192.
(32) (a) Oh, J. K.; Drumright, R.; Siegwart, D. J.; Matyjaszewski, K. *Prog. Polym. Sci.* **2008**, *33*, 448. (b) Jung, J.; Lee, I. H.; Lee, E.; Park, J.; Jon, S. *Biomacromolecules* **2007**, *8*, 3401. (c) Shi, L.; Khondee, S.; Linz, T. H.; Berkland, C. *Macromolecules* **2008**, *41*, 6546. (d) Hu, Y; Atukorale, P. U.; Lu, J. J.; Moon, J. J.; Um, S. H.; Cho, E. C.; Wang, Y.; Chen, J.; Irvine, D. J. *Biomacromolecules* **2009**, *10*, 756–765.
(33) (a) Stubbs, M.; McSheehy, P. M. J.; Griffiths, J. R.; Bashford, C. L. *Mol. Med. Today* **2000**, *6*, 15. (b) Torchilin, V. P. *Pharm. Res.* **2007**, *24*, 1. (c) Coakley, R. D.; Grubb, B. R.; Paradiso, A. M.; Gatzy, J. T.; Johnson, L. G.; Kreda, S. M.; O'Neal, W. K.; Boucher, R. C. *Proc. Natl. Acad. Sci. U.S.A.* **2003**, *100*, 16083.

Table 1. Recipes Used To Prepare Hybrid Nanogels

hybrid nanogels	St (mmol)	DVB (mmol)	AAPH[a] (mmol)	NIPAM (mmol)	AA (mmol)	BIS (mmol)	AAPH[b] (mmol)	yield[c] (%)	pH-induced swelling ratio $R_{h,swollen}/R_{h,shrunken}$ at 22 °C
pStNA1	0.52	0.21	0.02	7.51	0.66	0.39	0.08	~71	1.93
pStNA2	0.52	0.21	0.02	1.88	0.16	0.10	0.02	~93	2.67
pNA1				7.51	0.66	0.39	0.08	~92	1.97
pNA2				1.88	0.16	0.10	0.02	~97	2.01

[a] Used for initiating the polymerization of St and DVB. [b] Used for initiating the polymerization of NIPAM, AA, and BIS. [c] The number yield of core−shell hybrid nanogels as estimated from TEM observation.

a hydrophobic drug of dipyridamole (DIP) as a model to demonstrate the pH-triggered release. As expected, the nanogel shell can provide high loading capacity for such a generic drug without specific ligand modification. The resulting Ag-p(NIPAM-*co*-AA) core−shell hybrid nanogel delivery system could uptake DIP as high as 27.2% (w/w) (comparable to the loading in copolymer micelles[34]) and deliver a high cumulative amount of drug (20−80%, depending on the pH values). By tailoring the thickness, composition, and morphology of the nanogel shell in synthesis, not only the loading and releasing behavior of drugs can be modulated, but the interactions between the hybrid nanogels with cells can also be tuned, resulting in different cellular morphologies and selective cell staining. Moreover, the immobilization of the hydrogel shell on the surface of metal NPs may decrease the phagocytosis of the metal NPs and allow longer circulation time in blood.[35] The ability of the roboticized smart nanogel to provide long-circulation and specific accumulation, illuminate the targeted object, and intelligently dose the pathological zones will enable major advancements in diagnosis and therapy.

2. Experimental Section

Materials. Uranyl acetate ($UO_2(CH_3OCO)_2 \cdot 2H_2O$) was purchased from Electron Microscopy Sciences, and all other chemicals were purchased from Aldrich. NIPAM was recrystallized from a hexane−acetone (a 1:1 volume ratio) mixture and dried in vacuum. AA was purified by distillation under reduced pressure to remove inhibitors. DIP, silver nitrate ($AgNO_3$), sodium borohydrate ($NaBH_4$), L-ascorbic acid, HCl volumetric standard (0.1 N solution in water), sodium hydroxide (NaOH), sodium citrate ($Na_3C_6H_5O_7 \cdot H_2O$), styrene (St), divinylbenzene (DVB), *N,N*-methylenebisacrylamide (BIS), 2,2′-azobis(2-methylpropionamidine) dihydrochloride (AAPH), and cetyltrimethylammonium bromide (CTAB) were used as received without further purification. The water used in all experiments was of Millipore Milli-Q grade.

Synthesis of CTAB-Stabilized Ag NPs. Ag NPs were prepared through a seeded growth method, based on the reduction of $AgNO_3$ with ascorbic acid on CTAB stabilized Ag nanoparticle seeds. Ag seeds were prepared by dropwise addition of fresh $NaBH_4$ solution (5.3 mM, 0.5 mL) to an aqueous solution of $AgNO_3$ (0.1 mM, 40 mL) in the presence of sodium citrate (0.1 mM) under vigorous stirring. The resultant solution was stirred for 1 h and aged for 7 days at ambient condition before use. The long aging time is necessary for completely degrading the reducing powder of $NaBH_4$.[36] The growth of Ag NPs was carried out by addition of L-ascorbic acid solution (6 mL, 0.1 M) into a mixture of $AgNO_3$ (1.8 mM, 170 mL) and CTAB (19.9 mM) at 22 °C, followed by addition of the yellow seed solution (30 mL) and NaOH solution (1.0 mL, pH = 13.0) to adjust pH value. The resultant solution was stirred for 30 min. The Ag NPs were purified according to the method reported by Jana[37] to remove the nanorods and nanowires. The spherical Ag NPs were thus obtained by centrifugation (Thermo Electron Co. SORVALL RC-6 PLUS superspeed centrifuge) for 20 min at 5000 rpm and 36 °C, at which time the excess CTAB could be removed.

Synthesis of Smart Core−Shell Hybrid Nanogels with Ag NP as Core. Two types of hybrid nanogels were prepared according to the recipes listed in Table 1. In the first type of hybrid nanogels, the Ag NPs were initially coated with a thin layer of polystyrene (pSt) and then the copolymer gel layer of p(NIPAM-*co*-AA) was subsequently added. The precoating of pSt was performed as follows: as-prepared CTAB-stabilized Ag NPs were redispersed in 200 mL of deionized water in a 250 mL round-bottom flask equipped with a stirrer, a N_2 gas inlet, and a condenser. The solution was then heated to 30 °C, followed by addition of St and DVB under stirring. After 15 min, the temperature was raised to 70 °C and the polymerization was initiated by adding AAPH. The polymerization was allowed to proceed for 2 h. The solution was centrifuged twice at 5000 rpm (20 min) with the supernatant discarded and the precipitate redispersed in 60 mL deionized water. The resulting dispersion of pSt-coated Ag NPs was then purged with N_2, followed by addition of NIPAM, AA, and BIS. The mixture was heated to 70 °C. After 30 min, the polymerization was initiated with the addition of AAPH. The reaction was allowed to proceed for 4 h. The obtained hybrid nanogels were purified by centrifugation (5000 rpm, 20 min) and decantation and then washed with water three times. The resultant nanogels (60 mL) were further purified by 5 days of dialysis (Spectra/Por molecularporous membrane tubing, cutoff 12 000−14 000, the same below) against very frequently changed water at room temperature (~22 °C), and finally stored in a fridge (~3 °C). The obtained hybrid nanogels are coded as pStNA1 and pStNA2. The same synthetic and purification procedure was used to synthesize the second type of hybrid nanogels, in which no precoating of pSt was performed before adding the p(NIPAM-*co*-AA) copolymer gel layer to the surface of the Ag NP core. Only the mixture of NIPAM, AA, and BIS were used as the comonomers for polymerizations in the presence of CTAB-stabilized Ag NPs. The obtained hybrid nanogels are coded as pNA1 and pNA2.

Incorporation of the Hybrid Nanogels into Mouse Melanoma Cells, B16F10. Round glass coverslips were placed in each well of a 24-well plate and treated with 0.1% poly(L-lysine) in 100 mM PBS for 40 min. Following the treatment, the solution

(34) Tang, Y.; Liu, S. Y.; Armes, S. P.; Billingham, N. C. *Biomacromolecules* **2003**, *4*, 1636.
(35) Stolnik, S.; Illum, L.; Davis, S. *Adv. Drug Delivery Rev.* **1995**, *16*, 195.
(36) Chen, S.; Carroll, D. L. *J. Phys. Chem. B* **2004**, *108*, 5500.
(37) Jana, N. *Chem. Commun.* **2003**, 1950.

was aspirated and the wells were washed with PBS three times each. Next, B16F10 cells (2×10^4 cells/well) were plated on the glass coverslips at 80% confluence in DMEM containing 10% FBS and 1% penicillin-streptomycin. On the next day, each sample was diluted to three concentrations in serum-free DMEM in the following manner: (i) 50 μL of sample (0.75 μg) plus 450 μL of serum-free DMEM; (ii) 100 μL of sample (1.5 μg) plus 400 μL of serum-free DMEM; and (iii) 200 μL of sample (3 μg) plus 300 μL of serum-free DMEM. Additionally, 500 μL of serum-free medium was added to a control well. Each of the six diluted samples in a 500-μL medium was added to a marked well. The plate was incubated at 37 °C for 2 h. After 2 h, the medium was aspirated and fresh serum-free DMEM was added to each well. Finally, the coverslips with cells were removed from the wells and mounted onto slides with mounting fluid.

Drug Loading into the Hybrid Nanogels. A total of 3 mL of hybrid nanogels were redispersed in 20 mL of DIP solution (0.5 mg/mL, pH = 2.0). This suspension was stirred in an ice water bath for 4 h followed by an addition of NaOH solution to adjust the pH value to 11.0 and a continuous stirring for overnight. The DIP−nanogel complexes were then removed from the suspension by centrifugation at 5000 rpm and 22 °C for 30 min and redispersed in 50 mL of deionized water. The purification of the DIP-loaded hybrid nanogels was repeated by centrifugation and washing with deionized water several times. The final pH of the purified DIP-loaded hybrid nanogels was adjusted to 9.0. All the supernatant solutions of residual DIP were collected and dissolved adequately with 0.1 N HCl to form uniform solution. The concentration of free DIP was determined by fluorescence spectrometry at 480 nm with the excitation wavelength of 414 nm, based on the linear calibration curve with $R^2 > 0.99$ measured using the DIP solutions with known concentrations under the same condition. The loading content is expressed as the mass of loaded DIP drug per unit weight of dried hybrid nanogels.

In Vitro Drug Release Experiments. The release of DIP from the hybrid nanogels at 37 °C was evaluated by the dialysis method. A total of 1 mL of purified DIP-loaded hybrid nanogel dispersion was placed inside a dialysis bag immersed in 100 mL of 0.005 M PBS or HCl/PBS solutions of three different pH values at 7.38, 5.03, and 2.92, respectively. The released DIP outside of the dialysis bag was sampled at defined time periods and assayed by fluorescence spectrometry at 480 nm. Cumulative release is expressed as the total percentage of available drug released through the dialysis membrane over time.

In Vitro Cytotoxicity. B16F10 cells (2000 cell/well) were cultured in DMEM containing 10% FBS and 1% penicillin-streptomycin in a 96-well plate and exposed to free DIP, empty hybrid nanogels, and DIP-loaded hybrid nanogels. To cover the high concentrations, the nanogels were concentrated and adjusted to an appropriate concentration in DMEM right before feeding into the well. The plate was incubated at 37 °C for 2 h. The medium was then aspirated, and these wells were washed using fresh serum-free DMEM. After that, 25 μL of 3-(4,5-dimethyl-2-thiazolyl)-2,5-diphenyltetrazolium bromide (MTT) solution (5 mg/mL in PBS) were added to the wells. After incubation for 2 h, the solution was aspirated and 100 μL of DMSO was added to each well to dissolve the formazan crystal, and the plate was sealed and incubated overnight at 37 °C with gentle mixing. Cell viability was measured using a microplate reader at 570 nm. Positive controls contained no drug or nanogels, and negative controls contained MTT. Results are expressed as a percentage of the absorbance of the positive control.

Characterization. The FTIR spectra of the dried nanogels were recorded with a Nicolet Instrument Co. MAGNA-IR 750 Fourier transform infrared spectrometer. The UV−vis absorption spectra of the hybrid nanogel dispersions at different pH values were obtained on a Thermo Electron Co. Helios β UV−vis spectrometer. The PL spectra were obtained on a JOBIN YVON Co. FluoroMax-3 spectrofluorometer equipped with a Hamamatsu R928P photomultiplier tube, calibrated photodiode for excitation reference correction from 200 to 980 nm, and integration time of 1 s. The pH values were measured on a Mettler Toledo SevenEasy pH meter. TEM images were taken on a FEI TECNAI transmission electron microscope at an accelerating voltage of 120 kV. Approximately 10 μL of the diluted hybrid nanogel suspension was air-dried on a carbon-coated copper grid for the TEM measurements. The negative staining of the pSt/DVB-coated Ag NPs was performed as follows: a drop of the colloid was naturally desiccated on the TEM grid, and then a drop of 2% uranyl acetate in ethanol solution (prefiltered) was dripped on the copper grid for about 60 s and the extra droplet was removed and the grid dried prior to TEM observation. The B16F10 cells incubated with the hybrid nanogels in different concentrations and structures were respectively mounted on a clean slide, and imaged using a confocal laser scanning microscopy (LEICA TCS SP2 AOBS) equipped with a HC PL APO CS 20 × 0.7 dry lens. A UV (405 nm) light was used as the light source.

Dynamic light scattering (DLS) was performed on a standard laser light scattering spectrometer (BI-200SM) equipped with a BI-9000 AT digital time correlator (Brookhaven Instruments, Inc.). A He−Ne laser (35 mW, 633 nm) was used as the light source. All hybrid nanogel suspensions were passed through Millipore Millex-HV filters with a pore size of 0.80 μm to remove dust before the DLS measurements. In DLS, the Laplace inversion of each measured intensity−intensity time correlated function can result in a characteristic line width distribution $G(\Gamma)$.[38] For a purely diffusive relaxation, Γ is related to the translational diffusion coefficient D by $(\Gamma/q^2)_{C\to 0,q\to 0} = D$, where $q = (4\pi n/\lambda)\sin(\theta/2)$ with n, λ, and θ being the solvent refractive index, the wavelength of the incident light in vacuo, and the scattering angle, respectively. $G(\Gamma)$ can be further converted to a hydrodynamic radius (R_h) distribution by using the Stokes−Einstein equation, $R_h = (k_B T/6\pi\eta)D^{-1}$, where T, k_B, and η are the absolute temperature, the Boltzmann constant, and the solvent viscosity, respectively.

3. Results and Discussion

Synthesis of Hybrid Nanogels. The strategy to prepare the multifunctional hybrid nanogels with a copolymer hydrogel as shell and Ag NPs as the core involves first the synthesis of Ag NPs, followed by immobilization of an external stimuli-responsive hydrogel shell on the Ag NPs templates. The size of spherical Ag NPs synthesized with a seed-mediated growth method can be easily controlled by using a dilute CTAB solution at CTAB/Ag = 11.[36] The surfactant CTAB could assemble to form a bilayer at the surface of Ag nanocrystals.[36,39] The first monolayer binds with the ionic head groups pointed down toward the surface of Ag, and adsorption in this orientation is driven

(38) Chu, B. *Laser Light Scattering*, 2nd ed.; Academic Press: New York, 1991.
(39) Pérez-Juste, J.; Liz-Marzán, M.; Carnie, S.; Chan, D. Y. C.; Mulvaney, P. *Adv. Funct. Mater.* **2004**, *14*, 571.

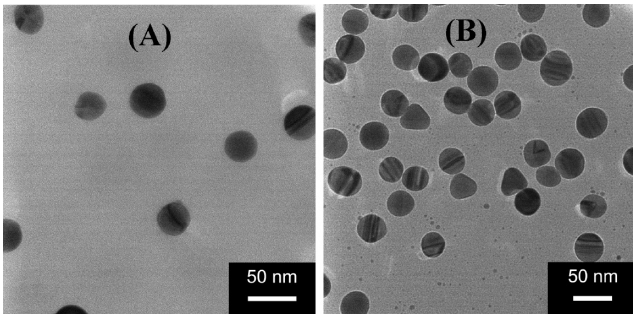

Figure 1. TEM images of (A) Ag NPs and (B) pSt-coated Ag NPs.

by the presence of chemisorbed bromide ions. The exposure of the alkyl chains to the aqueous solvent is energetically unfavorable, resulting in the adsorption of a second surfactant layer with the CTAB's head groups facing toward the water. In turn, the bilayer would provide additional stabilization and growth inhibition for Ag NPs. The Ag NPs are positively charged due to the coverage of a bilayer of the cationic surfactant CTAB.[39] Figure 1A shows the TEM image of spherical Ag NPs with an average diameter of 36 ± 3 nm. We have synthesized two groups of hybrid nanogels according to the recipes listed in Table 1. In one group of hybrid nanogels, the Ag NPs were precoated with a thin layer of polystyrene (pSt) cross-linked with DVB. A small amount of the St/DVB mixture was added to the Ag NP colloids stabilized with a CTAB bilayer adsorbed on the surface of Ag. The nearly water insoluble St and DVB monomers could only enter into the hydrophobic alkyl chain regions of the CTAB bilayer micelles. The in situ free radical polymerization and cross-linking of the St monomers with DVB resulted in a coverage of Ag NPs with a very thin layer of pSt chain network capped with CTAB molecules.[7a] Figure 1B shows a negative staining TEM image of the pSt-coated Ag NPs. The thin pSt shell can be observed as a white halo around each particle. The pSt shell provides the surface of the Ag NPs with nonpolymerized vinyl groups that are excellent anchor points for the subsequent copolymerization of NIPAM[7] and AA[40] in the presence of BIS as a cross-linker. The resulting hybrid nanogels with p(St-NIPAM-*co*-AA) as shell are coded as pStNA1 and pStNA2. In another group of hybrid nanogels, the nonmodified CTAB-capped Ag NPs were directly used for the free radical precipitation copolymerization of NIPAM and AA using BIS as a cross-linker. The resulting hybrid nanogels with p(NIPAM-*co*-AA) as shell are coded as pNA1 and pNA2. The synthesis of thermo-sensitive p(NIPAM-AA) microgels has been well established using the precipitation polymerization method. The p(NIPAM-AA) copolymer with 5−10 mol % AA has a lower critical solution temperature (LCST) below 50 °C under acidic condition.[40] Although the NIPAM and AA monomers are soluble in water, their copolymer of p(NIPAM-AA) chains have compact conformation and are water insoluble at temperatures above its LCST. In our synthetic process, the NIPAM, AA, and

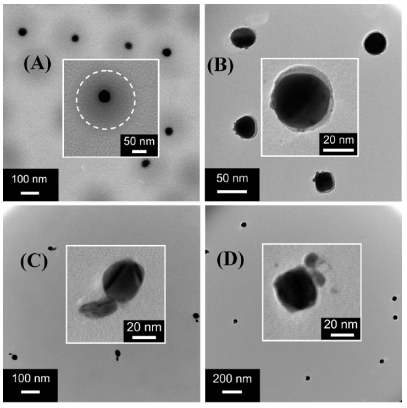

Figure 2. TEM images of hybrid nanogels: (A) pStNA1, (B) pStNA2, (C) pNA1, and (D) pNA2.

BIS monomers were uniformly dissolved in the water dispersion phase of Ag NP colloids stabilized with a CTAB bilayer. After the copolymerization was initiated at the reaction temperature of 70 °C, the hydrophobic p(NIPAM-AA) fragments formed at the early stage of reaction would nucleate and precipitate into the hydrophobic alkyl chain regions of the CTAB bilayer capping on the Ag NPs. While the copolymerization reaction proceeded, more p(NIPAM-AA) fragments were added onto the initially formed hydrophobic gel layer, leading to a continuous growth in size of the gel shell until the polymerization reaction was completed. The hybrid nanogel particles formed at 70 °C with Ag NP as core and p(NIPAM-AA) gel as shell were well dispersed in water as a result of the protection of CTAB layer. After being cooled down (below the LCST of gel shell), the p(NIPAM-AA) nanogel shell became hydrophilic, and CTAB was removed through the centrifugation, decantation, and dialysis.

Figure 2A,B shows the TEM images of the pStNA1 and pStNA2 hybrid nanogels with a clear core−shell structure having the Ag NP in the core and the p(St-NIPAM-*co*-AA) hydrogel uniformly coated on the Ag NP as shell. Two features should be noted. One is that the hydrogel shell in the pStNA1 sample is much thicker than that in the pStNA2 sample. Although the Ag NPs could offer enough contrast for imaging of the relative thin polymer layer due to their strong plasmon-enhanced absorption and high light-scattering ability,[41] a low contrast was observed on the polymer layer of pStNA1 and the core−shell structure is not so clear as the other types of nanogels, possibly due to the attenuated effect of Ag NPs across the thick polymer layer. Another is that small amount of free p(NIPAM-*co*-AA) copolymer gels (~30%) are presented in pStNA1 sample. As shown in Table 1, the ratio of commoners/Ag NPs in the feeding for synthesis of pStNA1 is four times higher than that for synthesis of pStNA2. These results indicated that the hydrogel shell thickness and the yield of Ag core−gel shell structured hybrid nanogels could be controlled

(40) Kratz., K.; Hellweg, T.; Eimer, W. *Colloids Surf., A* **2000**, *170*, 137.

(41) Xu, C.; Xie, J.; Ho, D.; Wang, C.; Kohler, N.; Walsh, E. G.; Morgan, J. R.; Chin, Y. E.; Sun, S. *Angew. Chem., Int. Ed.* **2008**, *47*, 173.

through the suitable selection of the monomers/Ag NPs feeding ratio in the synthesis. As observed in the pStNA2 sample, it is possible to minimize the formation of free polymer nanospheres and reduce the thickness of the hydrogel shell down to tens of nanometers at a low ratio of comonomers/Ag NPs. It should be mentioned that the number yield of the core−shell structured hybrid nanogels was determined from the counting method based on TEM observation. Three TEM images at different sample locations were taken for each type of hybrid nanogel. The average percentage of the Ag core−gel shell structured hybrid nanogels versus the total nanogels (containing both Ag core−gel shell structured and free polymer nanogels) was estimated. Figure 2C,D shows the TEM images of the pNA1 and pNA2 hybrid nanogels. Without the precoating of cross-linked hydrophobic pSt on the Ag NPs, the visor-like p(NIPAM-*co*-AA) copolymer gel shell covered asymmetrically on the Ag NP core in both pNA1 and pNA2 hybrid nanogels. In such morphology, part of the surface of the Ag NP core may only be covered with a very thin hydrogel layer. Similar asymmetric morphology was also observed in the Au-pSt hybrid colloidal particles synthesized from the precipitation polymerization of St in the presence of Au colloids.[42] Interestingly, the sizes of both pNA1 and pNA2 hybrid nanogels are small (e.g., below 100 nm), although the size of pNA1 is larger than that of pNA2 due to the higher feeding ratio of comonomers/Ag NPs for synthesis of pNA1. It should be noted that the size of colloidal drug carriers is very important to their fate in blood circulation since the recognition by the reticuloendothelial system (RES) is known to be the principal reason for the removal of many colloidal drug carriers from the blood compartment. The sub-200 nm size is desirable for colloidal drug carrier particles to extend their blood circulation time.[30] The size of the hybrid nanogels of pStNA2, pNA1, and pNA2 (Figure 2B−D) presented in this study is small enough to reasonably assume that they have high extravasation efficiency regardless of the cell type and conditions.

Volume Phase Transitions of Hybrid Nanogels. It is noteworthy that AA is a pH-responsive moiety, and the pH value of the dispersion medium can significantly influence the size of the hybrid nanogels. Figure 3 shows the pH-induced volume phase transitions of the hybrid nanogels, in terms of the change of hydrodynamic radius (R_h) measured at a scattering angle $\theta = 60°$ and temperatures of 22.1 °C (A) and 37.2 °C (B), respectively. A well-defined volume phase transition is observed for all the core−shell hybrid nanogels. When the pH was over the pK_a (≈4.2) of AA, the AA groups were gradually deprotonated. The Coulombic repulsion among the ionized carboxylate groups increased the osmotic pressure, resulting in the gradual increase in the size of the gel layer until all AA groups were deprotonated at pH > 5.5, where the hybrid nanogels reached a maximum swelling ratio (see Table 1). The size of the hybrid nanogels at 37.2 °C is

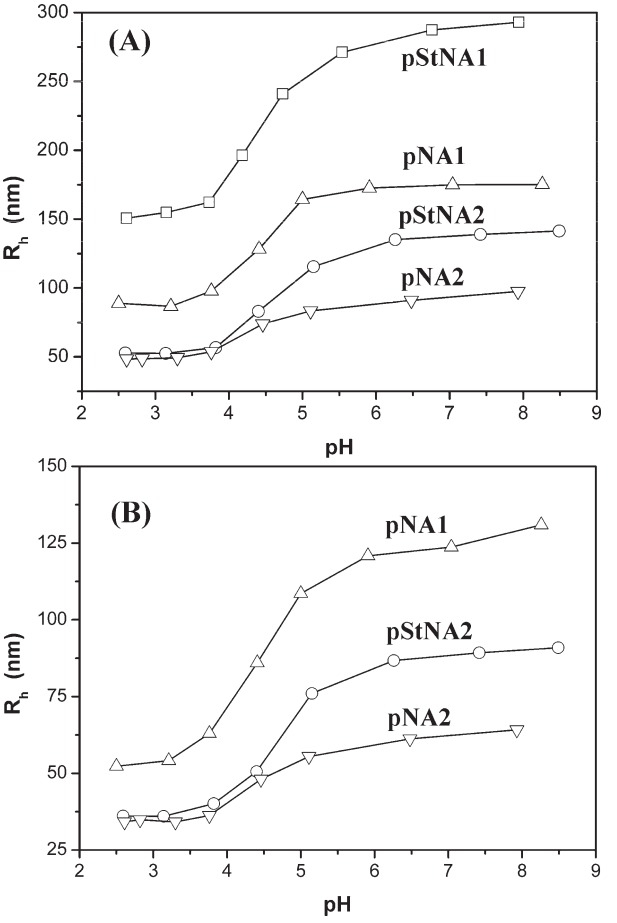

Figure 3. pH dependence of the average R_h values of different hybrid nanogels at a scattering angle $\theta = 60°$ and temperatures of (A) 22.1 °C and (B) 37.2 °C, respectively.

smaller than that at 22.1 °C due to the shrinkage of thermosensitive pNIPAM chain segments. It should be mentioned that the obtained hybrid nanogels are very stable. The volume phase transition curves of the hybrid nanogels were measured for three cycles with dialysis/pH adjustment, and all are reproducible and reversible. Since the measured curves are similar to that of a bare p(NIPAM-*co*-AA) microgel,[40,43] we can say that the presence of a metal core or pSt layer does not significantly affect the swelling behavior of the p(NIPAM-*co*-AA) gel shell. The pH-induced swelling/deswelling of the nanogel shell allows us not only to change the local surface environments of embedded Ag NPs to induce a pH-sensitive optical property but also to change the interaction degree between the drug and the gel network chains to control the drug release. Therefore, the core−shell hybrid nanogels presented in this work could offer two main advantages for the potential biomedical applications. The small size of hybrid nanogels with Ag NP core allows the deep penetration into cell/tissue such as poorly permeable tumors for labels and therapy, while the pH-responsive hydrogel shell can serve as excellent drug carriers with a pH-controllable drug releasing behavior.

(42) Ohnuma, A.; Cho, E. C.; Camargo, P. H. C.; Au, L.; Ohtani, B.; Xia, Y. *J. Am. Chem. Soc.* **2009**, *131*, 1352.

(43) Wu, W.; Zhou, T.; Zhou, S. *Chem. Mater.* **2009**, *21*, 2851.

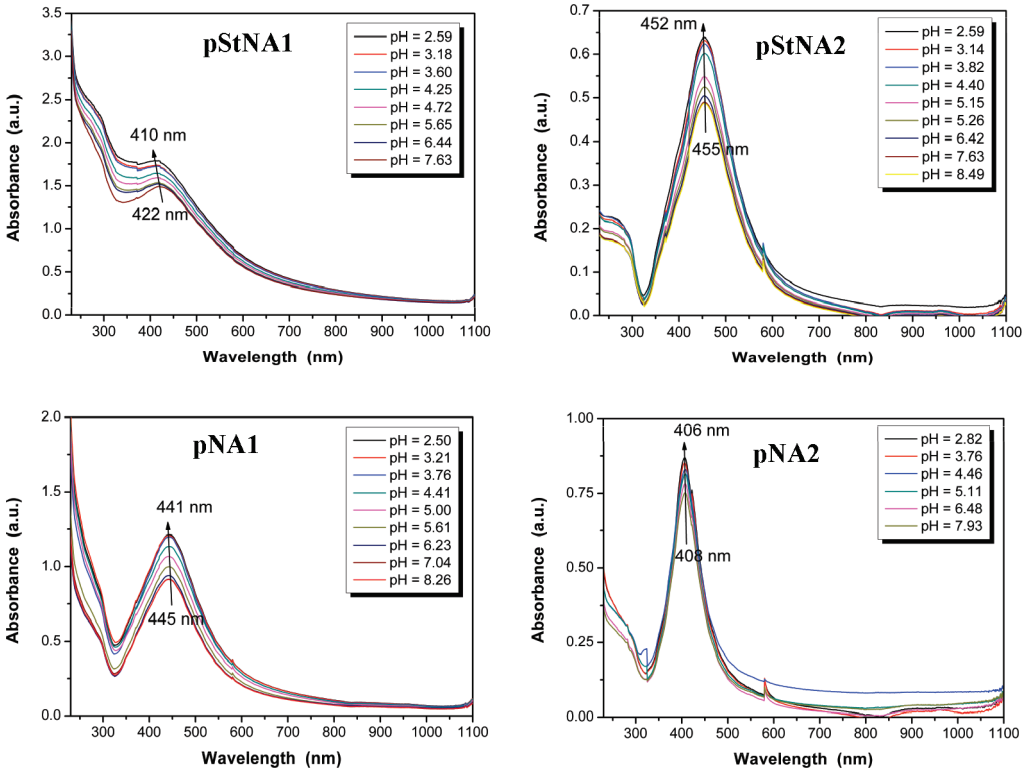

Figure 4. Effect of pH on the UV−vis absorption spectra of the four hybrid nanogels measured at room temperature.

pH-Sensitive UV−Vis Absorption Property of Hybrid Nanogels. Figure 4 shows the UV−vis absorption spectra of the four hybrid nanogels dispersed in aqueous solutions of different pH values. The Ag NPs (~36 nm) in the core of hybrid nanogels primarily absorb blue light, leaving the red and green light combined to give the dispersions a yellow color. The spectra showed two resonance peaks: the main dipole resonance peak at 400−460 nm, and a weak quadrupole resonance at 370 nm.[44] The dipole resonance arises from one side of the particle surface being positively charged and the opposite side being negatively charged, giving the particle itself a dipole moment that reverses sign at the same frequency as the incident light. The weak quadrupole resonance, characterized by two parallel dipoles of opposite sign, was induced by the energy losses that make the incident light nonuniform across the particle. Surface polarization is the most important factor in determining the frequency and intensity of plasmon resonance for a given metal because it provides the main restoring force for electron oscillation. On the other hand, the variation in the refractive index of the medium surrounding the particles could also change the position and intensity of the resonance peaks. For example, the thickness of the silica shell could change the surface plasmon resonance condition of the embedded Au NPs due to the corresponding changes in the local refractive index.[45,46] In our hybrid nanogels, the refractive index of the polymer gel shell is different from that of both the water and Ag core. The variation of pH values in the dispersion medium can swell or deswell the polymer gel shell, inducing a local refractive index change on the surface of the Ag NP core, which can further cause a change in the surface plasmon resonance of Ag NPs. As shown in Figure 4, when pH was decreased from ~8.5 (gel shell swollen) to 2.5 (gel shell collapsed) at room temperature, an increase in absorption intensity and a blue shift of the surface plasmon bands were observed for all the four hybrid nanogels. The enhancement of the surface plasmon band in the hybrid nanogels is likely attributed to the increase in the refractive index of the collapsed nanogel shell, which results in an increase of the Rayleigh scattering as previously reported and predicted by Mie theory.[45,46] The pH-induced blue shift of the resonance peaks could be attributed to many specific surface effects,[46] such as the solvent refractive index, the local refractive index surrounding the Ag NPs, and electron transfer.

Cellular Imaging. The fluorescence from noble metal NPs originates from radiative recombination of sp-band electrons and d-band holes, which could be enhanced by 4−6 orders of magnitude due to the surface plasmons of nanocrystals or rough metal surfaces.[10,20,21,47] Scaiano et al.[48] believed that the emission of Ag NPs are due to a small Ag cluster, predominantly Ag_2 supported by the readily detectable nanoparticles. Ag NPs of 28 ± 9 nm have shown strong fluorescence for cellular imaging.[20a] In our hybrid nanogels, the Ag NPs are coated with a smart

(44) Wiley, B. J.; Im, S. H.; Li, Z.; McLellan, J.; Siekkinen, A.; Xia, Y. N. *J. Phys. Chem. B* **2006**, *110*, 15666.
(45) Liz-Marzán, L. M.; Giersig, M.; Mulvaney, P. *Langmuir* **1996**, *12*, 4329.
(46) Mulvaney, P. *Langmuir* **1996**, *12*, 788.
(47) Boyd, G. T.; Yu, Z. H.; Shen, Y. R. *Phys. Rev. B* **1986**, *33*, 7923.
(48) Maretti, L.; Billone, P. S.; Liu, Y.; Scaiano, J. C. *J. Am. Chem. Soc.* **2009**, *131*, 13972.

hydrogel layer. To examine whether the luminescence properties of the Ag NP cores are preserved after being coated with the gel layer, confocal microscopy was used to take the luminescence images of the pStNA2, pNA1, and pNA2 hybrid nanogels dispersed on glass slides. Strong fluorescence was observed upon excitation with a UV laser of 405 nm or a blue laser of 488 nm using appropriate filter systems. After confirming the strong fluorescence, mouse melanoma cells B16F10 were incubated with the hybrid nanogels for observations of binding and morphological changes of the cancer cells.

Figure 5 shows the typical scanning confocal microscopy images of the B16F10 cells after being incubated with the pStNA2, pNA1, and pNA2 hybrid nanogels under three different concentrations of 1.5, 3.0, and 6.0 μg/mL, respectively. Controlled experiments were also carried out to make sure there was no significant autofluorescence from pristine cells under similar conditions. The smart nanogel can overcome cellular barriers to enter the intracellular region and light up the cells and even the nuclear regions. As the complexity of molecular interactions governing endocytosis are revealed, the mechanisms of endocytosis should be viewed in a broader context than simple vesicular trafficking.[8a] Recently, the surface-structure-regulated cell-membrane penetration by monolayer-protected Au NPs has been reported.[8b] While the NPs coated with subnanometer striations of alternating anionic and hydrophobic groups could penetrate the plasma membrane without bilayer disruption, the NPs coated with the same moieties but in a random distribution were mostly trapped in endosomes. The direct cell membrane penetration mechanism without overt bilayer disruption was also found for synthetic amphiphilic phospholipid polymers.[8c] In our systems, although the entrance mechanism of the hybrid nanogels into the cells is not clear, the surface properties of the hybrid nanogels should play a critical role in determining the outcome of their interactions with cells.[8] It is possible that the hybrid nanogel particles with both negatively charged carboxylate groups and hydrophobic polymer segments can penetrate the cell membrane without overt bilayer disruption. For pStNA2 hybrid nanogels, the p(St-NIPAM-*co*-AA) gel layer uniformly covers the core of the Ag NP. While the hydrophobic sites such as the backbone or grafted hydrocarbon chain segments in the gel could demonstrate a strong hydrophobic interaction with the hydrophobic cell membrane, including lipids and many proteins that aggregate at the plasma membrane, the negatively charged carboxylate groups in the gel shell would interact with the basic proteins that exist as positively charged moieties in the cytoplasm. Therefore, the pStNA2 hybrid nanogels could stain whole cell homogeneously and maintain the elongated cellular morphology with a green tint characteristic of illumination in the entire concentration range studied of 1.5−6 μg/mL. To identify the distribution of the pStNA2 hybrid nanogels in the cells, we have measured the transmission image and z-scan images from top to bottom for the selected sample area. Figure 6 shows the transmission image and z-scan

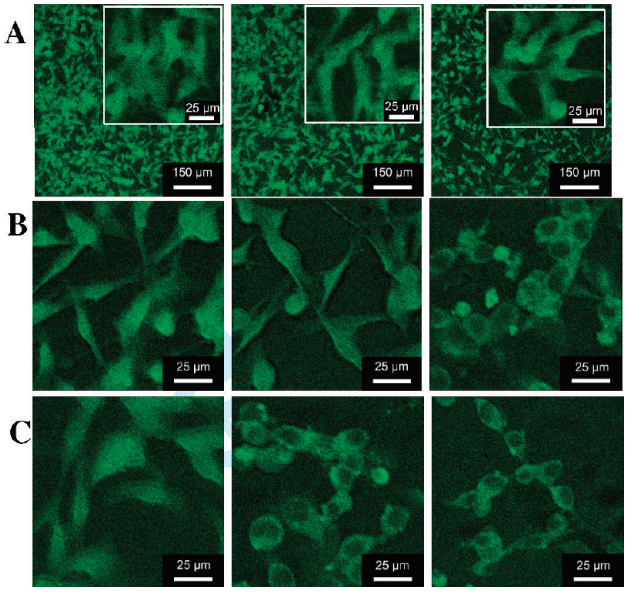

Figure 5. Scanning confocal images of B16F10 cells incubated with hybrid nanogels of pStNA2 (left), pNA1 (center), and pNA2 (right) at concentrations of (A) 1.5 μg/mL, (B) 3.0 μg/mL, and (C) 6.0 μg/mL, respectively. Excitation laser wavelength = 405 nm.

images of the B16F10 cells after being incubated with pStNA2 hybrid nanogels at 1.5 μg/mL. The transmission image shows that the hybrid nanogels with Ag NP as core are uniformly distributed in whole cells. The top-to-bottom z-scan images also indicate that the fluorescent hybrid nanogels are homogeneously distributed throughout the whole cell volume. However, for pNA1 and pNA2 hybrid nanogels, the elongated cellular morphology with fluorescence uniformly distributed in the whole cell was only observed at low concentration. When the concentration is increased to 6 μg/mL for pNA1 and 3−6 μg/mL for pNA2 hybrid nanogels, a more condensed and round shaped cellular morphology with a nonuniform distribution of the nanogel-associated fluorescence was observed. We speculate that the pNA1 and pNA2 hybrid nanogels may aggregate at relatively high concentrations after they interact with certain specific proteins in cells. As shown in Figure 2, the p(NIPAM-*co*-AA) gel layer is asymmetrically attached on the surface of Ag NP core in pNA1 and pNA2 (without the precoating of hydrophobic pSt). It is possible that part of the surface of the Ag NP core is only covered with very thin gel layer or even direct exposure to the cell, especially for the pNA2 sample with the total gel layer being designed very thin. The nonuniform polymeric gel coating with potential exposure of the metal surface in the pNA1 and pNA2 hybrid nanogels may provide additional charges from the Ag core surface to interact with certain specific proteins of the cytoplasm. At high concentrations of such structured hybrid nanogels, the hybrid nanogel−protein complexes may aggregate and induce a phase separation, resulting in nonuniform distribution of the hybrid nanogels in cells and more condensed and round morphology (see Supporting Information for transmission images, Figure S1). These results indicate that the structure and concentration of the core−shell hybrid nanogels could significantly affect

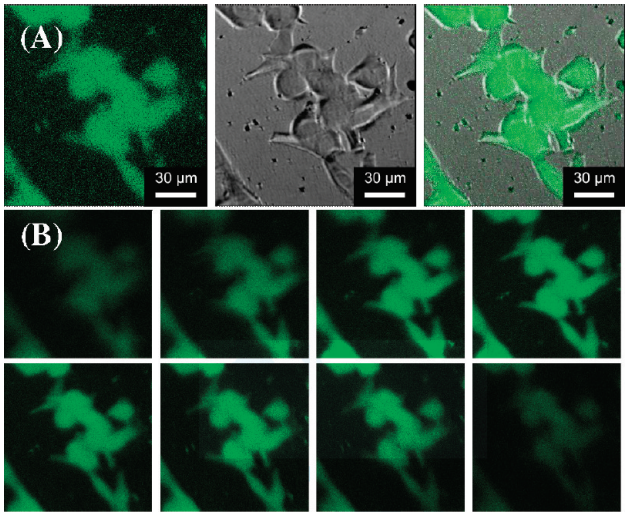

Figure 6. (A) Scanning confocal fluorescence (left), transmission (center), and overlaid images (right) of B16F10 cells incubated with hybrid nanogels of pStNA2 at a concentration of 1.5 μg/mL. (B) Cross-sectional Z-scan of a selected sample area (top to bottom). Excitation laser wavelength = 405 nm.

the cellular morphology due to the different interaction degrees between the nanogel and the cells. The round morphology at the high concentrations of the hybrid nanogel (3−6 μg/mL) should not be due to the unhealthy cells (see cytotoxicity in Figure 8). Similar morphology has also been observed on the B16F10 cells stained with other materials.[49] The discrete cellular morphologies at different structures and concentrations of the hybrid nanogels could potentially provide a handle to study the intracellular translocation processes. To the best of our knowledge, this is the first demonstration of core−shell hybrid nanogels with Ag NP as the core for cellular imaging. The coating of the gel layer on the Ag NPs and potential subsequent surface chemistry changes may not only increase the biocompatibility of Ag NPs but also provide cellular targeting ability.

Controlled Drug Release from Hybrid Nanogels. In addition to the function for cellular imaging, we expect that the pH-responsive hybrid nanogels should also provide another important function as drug delivery vehicles benefited from the stable network structure under different conditions. DIP, a known platelet inhibitor, coronary vasodilator,[50] and a coactivator of antitumor compounds,[51] was chosen as the model drug to study the loading and releasing behavior of the hybrid nanogels. As a water−poorly soluble weak base ($pK_a \sim 6.4$), DIP dissolves readily in acidic solution but incompletely in basic solution. In a blank experiment, DIP dissolved very well and formed a transparent yellow

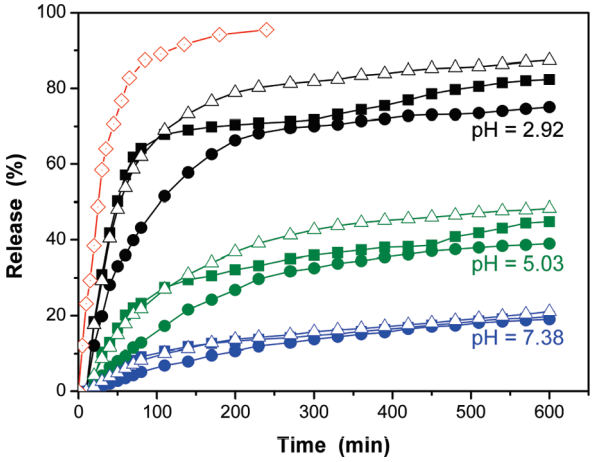

Figure 7. Releasing profiles of DIP from the pStNA2 (■), pNA1 (●), and pNA2 (△) hybrid nanogels in PBS solutions of different pH values at 37 °C. In the blank release (◇), 1 mL of 0.032 mg/mL DIP solution without nanogels was released to 100 mL of PBS buffer at pH = 2.92.

solution in an acidic solution of pH = 2.0. As the pH was raised to above pK_a (e.g., pH = 11.0), the DIP precipitated immediately as fine particles and made the solution cloudy yellow. In the presence of hybrid nanogels, the hybrid nanogel−DIP complex solution was somewhat translucent at pH = 11.0, but no evident precipitate was observed. The swollen p(NIPAM-*co*-AA) gel layer under the basic conditions can provide a large mesh size to trap the insoluble DIP drug in either a molecular or a nanocrystalline state through the hydrophobic interactions between the hydrophobic sites of DIP and polymer chains as well as the hydrogen bonding interactions between the hydroxyl groups on DIP and the amide groups on polymer chains, which can result in a high drug loading capacity. The yields of DIP loaded into the hybrid nanogels were determined to be 19.3, 27.2, and 11.3% (w/w) for pStNA2, pNA1, and pNA2, respectively, which is comparable to the loading capacity of copolymer micelles.[34] The pNA1 hybrid nanogels possess a much thicker polymeric gel layer coated on the Ag NP core than the pNA2, so the pNA2 sample can load much more of the DIP drug. For pStNA2 sample, although the coated hydrogel layer is very thin (same amount of feeding as pNA2), the hydrophobic inner PS layer can provide additional hydrophobic domains to uptake the hydrophobic DIP molecules or nanocrystallines. Therefore, the pStNA2 sample can load more DIP drug compared to the pNA2 sample. It should be mentioned that the confocal microscopy images of the DIP-loaded nanogels still demonstrate a strong fluorescence.

Figure 7 shows the cumulative release profiles of DIP from the pStNA2, pNA1, and pNA2 hybrid nanogels into buffer solutions measured by a conventional dialysis bag method at a physiological temperature of 37 °C and different pH values, respectively. A blank release experiment from the free DIP solution with the equivalent amount of drug (0.032 mg/mL) to that trapped in the pNA2 hybrid nanogels was performed at pH 2.92 for comparison. Clearly, the DIP release from the free DIP solution is much faster than from the hybrid nanogels.

(49) (a) Sahoo, A.; Jung, Y. M.; Kwon, H.; Yi, H.; Lee, S.; Chang, S.; Park, Z.; Hwang, K.; Im, S. *J. Biol. Chem.* **2008**, *283*, 28860. (b) Wu, W.; Aiello, M.; Zhou, T.; Berliner, A.; Banerjee, P.; Zhou, S. *Biomaterials* **2010**, doi: 10.1016/j.biomaterials.2010.01.011.
(50) Marchandt, E.; Prichard, A. D.; Casanegra, P.; Lindsay, L. *Am. J. Cardiol.* **1984**, *53*, 718.
(51) (a) Shalinsky, D. R.; Jekunen, A. P.; Alcaraz, J. E.; Christen, R. D.; Kim, S.; Khatibi, S.; Howell, S. B. *Br. J. Cancer* **1993**, *67*(1), 30. (b) Hejna, M.; Raderer, M.; Zielinski, C. C. *J. Natl. Cancer Inst.* **1999**, *91*, 22.

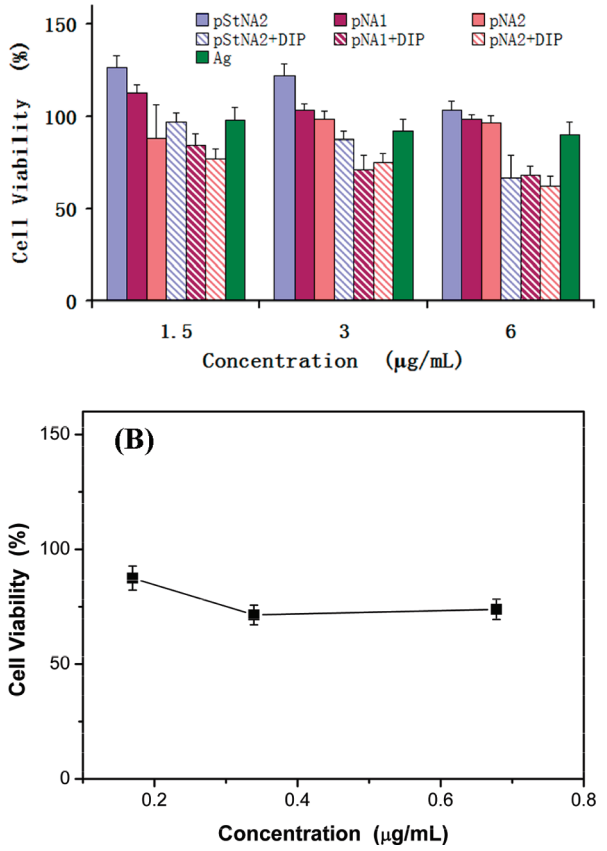

Figure 8. (A) In vitro cytotoxicity of empty pStNA2, pNA1, and pNA2 hybrid nanogels and DIP-loaded pStNA2, pNA1, and pNA2 hybrid nanogels against B16F10 cells. The control experiment on the Ag seed NPs and free DIP solution (B) was presented for comparison. The concentrations of DIP used for the control study are equal to DIP loaded in the interior of the pNA2 hybrid nanogels correspondingly.

In the absence of hybrid nanogels, 82% of the total DIP loaded into the dialysis bag was burst released in the first hour, which indicates that the DIP molecules can permeate through the dialysis membrane easily. In contrast, it takes a much longer time to release the same amount of DIP from the hybrid nanogels. Even for the pNA2 sample with thinnest gel layer and fastest releasing rate, it needs about 6 h to release 80% of the total loaded DIP. This retardation indicates that the DIP drug trapped in the networks of hybrid nanogels were released in a controlled manner.

Two features should be noted from the controlled release of DIP from the hybrid nanogels. First, the pH of external buffer solution can trigger the DIP releasing rate. The decrease in pH increases the DIP releasing rate from all the hybrid nanogels. When the drug-loaded hybrid nanogels were placed in a pH 7.38 buffer, only ~20% of the loaded DIP could be released even after 10 h. When the pH of the external buffer solution was decreased to 5.03, about 35−40% of the loaded DIP could be released within 10 h. When the pH was further decreased to 2.92, about 75−85% of the loaded DIP could be released in 10 h. We think that both the pH-sensitive solubility of DIP drug and the pH-sensitive swelling degree of the p(NIPAM-*co*-AA) gel layer are important to induce the pH-controllable drug release. On the one hand, the decrease in pH (e.g., <5.0) greatly increases the solubility of DIP. On the other hand, the decrease in pH (e.g., <4.0) induces the collapse of the p(NIPAM-*co*-AA) gels due to the protonated carboxylic groups in AA units. The shrinkage of the gel network can expel the soluble guest DIP molecules, thus significantly improving the releasing rate of the DIP drug. Second, the tailoring of the shell thickness and structure of the hybrid nanogels can also modify the DIP releasing profiles to a certain extent. The thicker the gel shell, the slower the DIP releasing rate. For example, pNA1 hybrid nanogels have the same morphology and composition but a thicker gel shell in comparison with pNA2, resulting in a slower DIP releasing rate due to the longer restricted diffusion path in the thick gel shells. For pStNA2 hybrid nanogels, the Ag NP core was precoated with a thin hydrophobic pSt layer before adding the same amount of p(NIPAM-*co*-AA) gel layer as in the pNA2 sample. The additional inner pSt layer in the nanogel shell not only increases the DIP loading capacity but also slows down the DIP releasing rate. More interestingly, the pStNA2 hybrid nanogels with double polymer layers in the shell exhibited a clear two-stage release at acidic pH values, while pNA1 and pNA2 hybrid nanogels with p(NIPAM-*co*-AA) gel only as the shell demonstrated only a single stage release kinetics. For example, the pStNA2 nanogels undergo a large degree of release in the first 200 min, followed by a second burst with a smaller degree of release starting at around 450 min at pH = 5.03, and 300 min at pH = 2.92, respectively. The mechanism of the two-stage release kinetics is not quite clear. We believe that the shell structure with double layers of different polymer compositions is responsible for the two-stage releasing behavior. In the pStNA2 hybrid nanogels, the shell coated on the Ag NP core is composed of a relatively hydrophobic pSt inner layer and a relatively hydrophilic p(NIPAM-*co*-AA) hydrogel periphery. It is possible that only after the DIP incorporated in the peripheral p(NIPAM-*co*-AA) layer was released to certain degree, the DIP solubilized in the endothelial pSt layer could diffuse out through the p(NIPAM-*co*-AA) gel periphery to be released. It should be noted that no two-stage release kinetics was observed from the same pStNA2 nanogels at pH = 7.38 in our experimental time window, which may be due to the insufficient releasing of DIP in the peripheral p(NIPAM-*co*-AA) layer for DIP trapped in the inner pSt layer to diffuse out. We therefore present a series of novel hybrid nanogels for not only the pH-triggered drug release but also the tunable gradient release through the tailoring of the nanogel shell composition and structure coated on the surface of the Ag NP core. Although DIP was used as a drug model in the present study, it is expected that the pH-responsive hybrid nanogel system can be applied to other hydrophilic or hydrophobic drugs that do not exhibit a pH-dependent solubility because the variation in pH will not change the overall release mechanism of drugs trapped in the gel networks (see Supporting Information SI2 and Figure S2).

In Vitro Cytotoxicity. For future biological applications, materials should be non- or low-cytotoxic. As shown in Figures 5 and 6, no signs of morphological damage to the cells were observed upon treatment with hybrid nanogels, thereby demonstrating their minimal cytotoxicity. To further evaluate the cytotoxicity of the hybrid nanogels, in vitro cytotoxicity tests were elaborately conducted against B16F10 cells. The potential cytotoxicity of the free Ag NPs with the corresponding concentrations was also addressed. As shown in Figure 8, the empty hybrid nanogels and free Ag NPs were non- or low-cytotoxic to B16F10 cells in concentrations of up to 6 μg/mL. These results confirm that the discrete cellular distribution of hybrid nanogels shown in Figure 5 could be due to their intracellular translocation processes, rather than the toxicity. Surprisingly, the cell viability drastically decreased when the cells were incubated with DIP-loaded hybrid nanogels even at a concentration as low as 1.5 μg/mL (equivalent to about 0.17 μg/mL free DIP). The cytotoxicity of DIP-loaded hybrid nanogels is higher than that of free hybrid nanogels in all the studied concentrations. DIP is a known coactivator of antitumor compounds, and the formation of metastatic tumors could be inhibited by such inhibitors of platelet aggregation.[51] Despite of these encouraging preliminary results and a compelling biochemical rationale, we cannot conclude weather the DIP-loaded hybrid nanogels would be pharmacologically active for cancer treatment because very limited information exists on the clinical use of anticoagulants for the prevention or treatment of cancer.[51b] Nevertheless, the increase in cytotoxicity in the presence of DIP-loaded hybrid nanogels can be attributed to the cellular uptake of DIP-loaded hybrid nanogels and possibly their sustained-release property.

4. Conclusions

Core−shell structured hybrid nanogels composed of Ag NP as core and pH-responsive copolymer gel of p(NIPAM-*co*-AA) as shell with different shell thickness and structure can be successfully synthesized from the precipitation polymerization of NIPAM and AA onto the colloidal Ag NPs. While the pSt precoated Ag NPs produce a uniform coverage of the polymer gel shell, the nonmodified CTAB-capped Ag NPs produce an asymmetric coverage of the polymer gel shell. The gel shell thickness can be controlled through the feeding ratio of comonomer/Ag NP. The decrease in pH can induce an increase in absorption intensity and a blue shift of the surface plasmon bands of the Ag NP due to the refractive index change surrounding the Ag NP core when the gel shell shrinks. The smart nanogel can overcome cellular barriers to enter the intracellular region and light up the mouse melanoma B16F10 cells and even the nuclear regions. While the network structure of the gel shell can provide high loading capacity for a generic hydrophobic DIP drug, the pH-responsive swelling degree of the gel shell can trigger the drug release and thereby may enhance the therapeutic efficacy of the drugs under the local stimuli of the target pathological zone such as cancer and cystic fibrosis that are associated with disruptions in acid/base homeostasis. The thickness, composition, and structure of the nanogel shell can not only modulate the drug loading and releasing behavior but also tune the interactions between the hybrid nanogels with cells, resulting in different cellular morphologies and selective cell staining. Furthermore, the surface carboxyl groups on the hybrid nanogels can be potentially used for further bioconjugation for targeting function. Such a novel type of multifunctional core−shell structured hybrid nanogel materials may find important biomedical applications.

Acknowledgment. We gratefully acknowledge the financial support from the U.S. Agency for International Development under the U.S.-Pakistan Science and Technology Cooperative Program (PGA-P280422) and the National Science Foundation (CHE 0316078). We also thank Dr. Yalin Wang at the imaging facility center of CUNY-CSI for his kind support on the TEM and confocal microscopy experiments.

Supporting Information Available: Transmission images of the selected sample area of the B16F10 cells after being incubated with a hybrid nanogel of pNA2 at a concentration of 3.0 μg/mL, and the analysis of drug release mechanism on the basis of the Peppas empirical equation (PDF). This material is available free of charge via the Internet at http://pubs.acs.org.